agriculture

MDPI

Article

Design, Integration, and Experiment of a Multi-Variety Rice Seedling Transplanting Robot with a Force–Position-Controlled Rigid–Flexible Coupled End Effector

Chao Kong, Yaoyun Wu, Runxin Zhang, Qingyu Zhang, Zhenxing Su and Di Yu *

College of Mechanical and Electrical Engineering, Northeast Forestry University, Harbin 150040, China
* Correspondence: yudi.1986@hotmail.com

Abstract

To address the high labor intensity, low efficiency, and unstable precision of manual transplanting in rice breeding experimental fields—where conventional transplanters fail to meet the operational requirements—an intelligent transplanting robot for multi-variety rice seedlings was designed. Based on an analysis of the agronomic parameters of rice seedling transplanting, an integrated system architecture consisting of a tracked mobile chassis, a six-degree-of-freedom collaborative robotic arm, and a custom-designed end effector was constructed. A bionic rigid–flexible coupled end effector was developed, and a force–position closed-loop control strategy was established. The YOLOv5s algorithm combined with distinct-color auxiliary markers was adopted to achieve rapid recognition of multi-variety rice seedlings, and hand–eye calibration was used to realize pose transformation. Forward and inverse kinematics analyses were conducted to verify the reachability of the workspace. Finally, a multi-variety rice seedling transplanting test bench was built to validate the robot's performance. The results showed that the rice seedling transplanting success rate reached 94.90%, the transplanting accuracy rate reached 97.96%, the average damage rate was only 3.06%, and the transplanting time was 7.85 s per hill. All metrics satisfied the requirements of breeding trials for operational accuracy and data consistency.

Keywords: intelligent transplanting robot; rigid–flexible coupling; force–position control; YOLOv5s; kinematics analysis

1. Introduction

Rice is the primary staple food crop in China and a cornerstone of global food security, and its stable and increased production is directly linked to global food security and sustainable agricultural development [1,2]. Rice breeding is the core means of improving yield, grain quality, and stress resistance [3]. As a critical procedure in breeding trials, seedling transplanting directly determines the accuracy of variety screening and the reliability of field trial data through its operational precision and consistency [4,5]. Currently, transplanting operations in rice breeding experimental fields remain predominantly manual, giving rise to prominent problems such as high labor intensity, low efficiency, high cost, and unstable precision [6]. Moreover, as the global agricultural workforce ages, labor shortages have become a major bottleneck constraining the development of large-scale precision breeding [7]. Meanwhile, commercial transplanters are designed for large-scale operations on single-variety paddy fields, adopting a standardized working mode with fixed row and hill spacing [8]. They cannot rapidly switch variety parameters, and their large turning radius and poor field adaptability render them entirely unsuitable for the small-plot,

Check for updates

Academic Editor: Wei Ji

Received: 10 September 2026
Revised: 21 October 2026
Accepted: 29 October 2026
Published: 2 November 2026

Copyright: © 2026 by the authors. Licensee MDPI, Basel, Switzerland. This article is an open access article distributed under the terms and conditions of the Creative Commons Attribution (CC BY) license.

multi-variety, and high-precision operation scenarios of breeding experimental fields [9,10]. Therefore, developing an intelligent transplanting robot adapted to the refined operation requirements of rice breeding experimental fields holds significant engineering value and scientific importance for enhancing the automation level of rice breeding, ensuring the reliability of trial data, and advancing the development of the modern seed industry [11].

In recent years, driven by the rapid advances in robotics, artificial intelligence, and sensing technologies, significant progress has been made in the intelligent development of rice transplanting equipment [12,13]. In the field of navigation and control, Lohan et al. [14] designed a remote control system for a two-wheel rice transplanter based on virtual reality/augmented reality. By integrating an autonomous driving controller with a real-time kinematic global navigation satellite system (RTK-GNSS) module, the system achieved operation path visualization and remote operation, addressing the safety issues of manual driving in hot and muddy paddy field environments. Wu et al. [15] proposed a visual–inertial fusion pose estimation scheme. By fusing visual and inertial navigation information through joint sensor calibration and the extended Kalman filter (EKF) algorithm, the scheme addressed the problems of satellite positioning being susceptible to interference and the insufficient robustness of a single sensor. He et al. [16] constructed a positioning correction model based on implement attitude. By indirectly obtaining the center pose of the implement through coordinate system transformation and Kalman filtering, the model resolved the trajectory inconsistency caused by relative pose changes between the vehicle body and the implement. In terms of operating mechanism optimization, Siddique et al. [17] established a temperature–viscosity dynamic characteristic model of the hydraulic proportional valve. Based on the proportional–integral–derivative (PID) control algorithm, they optimized the response speed of the valve control system, thereby improving the control accuracy of the transplanter's seedling-picking mechanism. Zhou et al. [18] designed a three-transplanting-arm mechanism constrained by a differential non-circular gear train. Through single-stage non-uniform transmission constraining the 2R open-chain motion, the mechanism resolved the problems of low transplanting accuracy and poor trajectory attitude caused by the accumulation of backlash in multi-stage transmission. However, research on conventional transplanters has consistently focused on large-scale paddy field operations. Although these technical optimizations have significantly improved the efficiency and accuracy of large-scale transplanting, they generally suffer from limitations in scenario adaptability and can hardly meet the operational requirements of breeding experimental fields.

Meanwhile, in the field of agricultural robotics, the "mobile chassis + robotic arm + end effector" configuration has been widely studied and applied in fruit and vegetable picking scenarios [19]. In terms of end effectors, Silwal et al. [20] designed a seven-degree-of-freedom apple-picking robot equipped with a three-finger tendon-driven end effector, achieving a harvesting success rate of 84% in field trials. Xiong et al. [21] developed a tendon-driven strawberry-picking gripper with a six-finger structure comprising three active fingers and three passive covering fingers that "swallow" the fruit from below. Built-in sensors correct positional errors, addressing the problems of strawberry susceptibility to damage and the difficulty of separating clustered fruits, with a success rate of 96.8% for isolated strawberries. In terms of rigid–flexible coupling structures, Yang et al. [22] designed a tomato-picking end effector with a retractable suction cup, addressing the problem of low picking success caused by interference from branches and leaves. Field validation achieved a harvesting success rate of 88% with a per-fruit harvesting time of 5.4 s. However, existing end effectors of agricultural robots are mostly designed for spherical fruits or vegetable plug seedlings, which are incompatible with the morphology of rice seedlings and the requirements of paddy field transplanting. Moreover, existing studies

generally focus on low-damage grasping of a single variety and lack adaptive grasping and quantitative seedling-picking control methods for multi-variety rice seedlings.

In summary, rice transplanting in breeding experimental fields faces the dual challenges of labor shortages and poor manual operation precision, which directly affect the reliability of trial data. To address these problems, this study took the bowl-shaped carpet seedlings from breeding experimental fields in the cold-region black soil reclamation area as the research object and designed an intelligent transplanting robot for multi-variety rice seedlings. A bionic rigid–flexible coupled end effector adapted to multi-variety rice seedlings was developed, and, combined with force–position closed-loop control, it achieved low-damage quantitative grasping. A vision-based recognition and positioning system was constructed simultaneously, and forward and inverse kinematics analyses of the intelligent transplanting robot were conducted in MATLAB R2022b software to solve its workspace. Finally, a multi-variety rice seedling transplanting and picking test bench was built, verifying that all indicators of the intelligent transplanting robot met the primary requirements for operational precision and data consistency in breeding experiments.

2. Materials and Methods

2.1. Agronomic Parameters of Rice Seedling Transplanting

This study was conducted in the breeding experimental fields of the Jiansanjiang Reclamation Area in Heilongjiang Province. The region has a cold-temperate continental monsoon climate. During the rice transplanting period, the ambient temperature ranges from 5 to 31 °C, the maximum solar irradiance can reach 1000 W/m^2, the soil water content is 25–30%, and the field surface exhibits a micro-slope of $\leq 5^\circ$ [23]. The research object was the bowl-shaped carpet seedling, raised in a specialized seedling tray with a matrix arrangement of bowl cavities. The individual bowls were lightly interconnected through a thin layer of substrate or slight root entanglement, which facilitated quantitative seedling picking by the end effector [24].

According to the operation standards for rice transplanters and the specific specifications for breeding experiments, combined with actual production requirements, the core agronomic parameters of rice seedling transplanting were determined. Four different varieties of mature rice seedlings with uniform growth were selected from the experimental fields. For each variety, three trays of seedlings at the appropriate transplanting stage were randomly selected, and 30 samples were taken from each tray, yielding a total of 360 valid samples (independent samples, used exclusively for measuring the physical parameters of rice seedlings). A ruler (accuracy 1 mm), a digital vernier caliper (accuracy 0.01 mm), an electronic balance (accuracy 0.01 g), and a digital push–pull force gauge (accuracy 0.01 N) were used to measure the core physical parameters of the rice seedlings. The statistical results of the two types of parameters are shown in Table 1.

Table 1. Values of agronomic parameters for rice seedling transplanting.

Name	Project	Indicators
Standards for transplanting rice seedlings	Row spacing (cm)	30 ± 5
	Plant spacing (cm)	13 ± 1
	Transplanting depth (cm)	2 ± 0.5
	Number of seedlings per hole (plant)	4 ± 1
Physical parameters of rice seedlings	Plant height (cm)	16.3
	Diameter of the root ball with soil (mm)	2.43
	Weight of a single plant with soil (g)	0.32
	Vertical uplift force per plant (N)	0.14

2.2. Overall Design of the Robot System

According to the operational requirements of rice breeding experimental fields and based on the agronomic parameters of rice seedling transplanting, three overall design objectives were determined for the robot: multi-variety adaptability, high-precision operation, and low-damage transplanting. An integrated operation system consisting of a "mobile chassis + robotic arm + custom-designed end effector" was constructed to achieve precise and automated transplanting. The overall structure of the intelligent transplanting robot for multi-variety rice seedlings is shown in Figure 1, which mainly consists of a mobile chassis, a robotic arm, an end effector, a seedling tray rack, seedling trays, a depth camera, and a light detection and ranging (LiDAR) sensor.

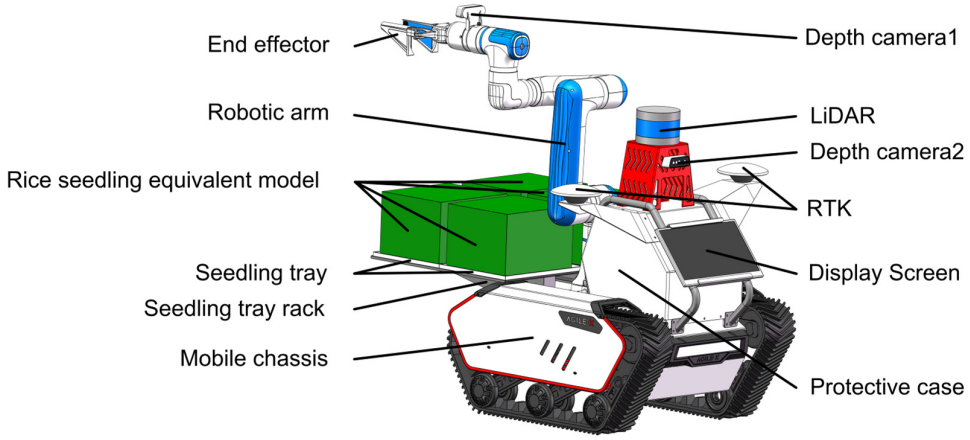


Figure 1. Schematic diagram of the intelligent transplanting robot for multi-variety rice seedlings.

The tracked chassis serves as the mobile platform of the intelligent transplanting robot for multi-variety rice seedlings. A LiDAR, a depth camera, an inertial measurement unit (IMU), and an RTK positioning module are integrated at the front of the tracked chassis, forming a complete navigation and positioning system. A protective enclosure housing the onboard computer and battery pack is mounted on the mobile chassis. The robot adopts a six-axis robotic arm as the core operation actuator, assisting the end effector in completing the rice seedling transplanting operation. Equivalent models of the four different rice seedling varieties are placed in four seedling trays of uniform size, and the trays are arranged in an orderly manner on a seedling tray rack rigidly connected to the mobile chassis. Specifically, depth camera 2 is mounted at the front of the mobile chassis, where it senses the field environment ahead and captures images and depth data to support the autonomous driving of the mobile chassis; depth camera 1 is mounted at the end of the robotic arm, where it senses the rice seedlings in the trays and captures images and depth data to support visual recognition and positioning.

The transplanting workflow of the intelligent transplanting robot for multi-variety rice seedlings is shown in Figure 2. Through the theoretical design scheme of multi-sensor fusion simultaneous localization and mapping (SLAM), the mobile chassis realizes mapping of the experimental field and centimeter-level positioning and navigates autonomously to the target working area; upon arrival, the mobile chassis stops and the manipulator returns to its preset initial position. The transplanting operation follows a closed-loop workflow of "recognition–grasping–transporting–planting–reset". The depth camera captures images, and the target pose of the rice seedling is obtained through visual recognition and hand–eye calibration. The robotic arm moves the end effector to the grasping point and completes damage-free grasping based on pressure-feedback closed-loop control. The seedling is then transported to the preset planting point for planting, and the robotic arm resets to the

standby position. After completing operations in one area, the mobile chassis autonomously navigates to the next area until all tasks are finished.

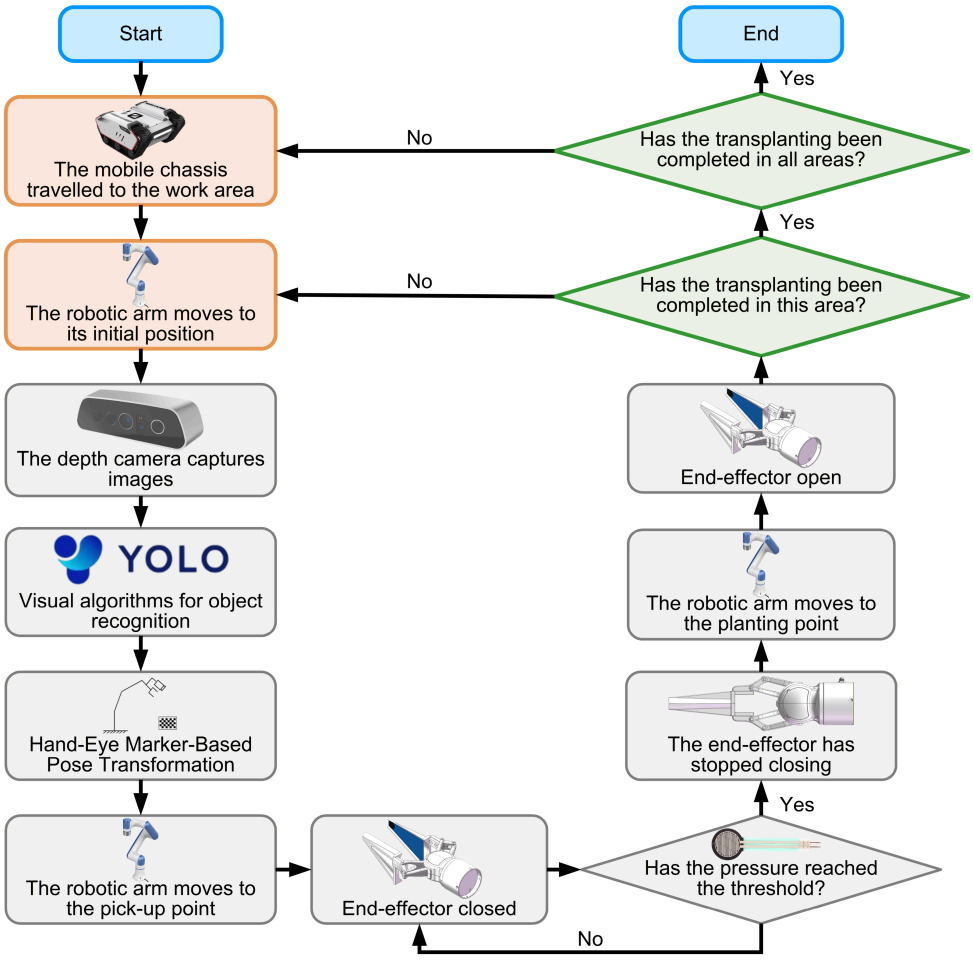


Figure 2. Transplanting workflow of the intelligent transplanting robot for multi-variety rice seedlings.

2.3. Selection of the Mobile Chassis and Robotic Arm

The mobile chassis and robotic arm constitute the core hardware platform of the robot, whose performance directly determines the operational precision, adaptability, and reliability of the entire machine. The mobile chassis must provide centimeter-level absolute positioning accuracy and trajectory tracking capability to ensure clear operational boundaries. It should have an extremely small turning radius to adapt to irregular small-area experimental fields, rely on wide tracks or special wheeled structures to improve anti-sinking capability in paddy fields, and be equipped with sufficient ground clearance and climbing capability to cope with complex terrain. In addition, it must possess load-bearing capacity sufficient for the total machine load and an ingress protection rating of no less than IP67 to ensure operational stability and reliability.

The robotic arm must possess centimeter-level positioning accuracy to meet the stringent precision requirements of hill spacing, row spacing, and transplanting depth in the experimental fields. Its workspace must fully cover the entire transplanting operation range, and its payload capacity must match the total weight of the end effector and rice seedlings. Its structure should balance light weight and rigidity, with the protection rating of key components no less than IP67, ensuring stable and reliable operation of the entire machine. Based on the above requirements, this study selected the BUNKER MINI tracked mobile chassis (AgileX Robotics, Shenzhen, China) and the Nova 2 six-axis robotic arm

(Dobot, Shenzhen Yuejiang Technology Co., Ltd., Shenzhen, China), whose core parameters are listed in Table 2.

Table 2. Performance parameters of the mobile chassis and robotic arm.

Name	Project	Indicators
Bunker mini	Ground clearance (mm)	80
	Dynamic load (kg)	25
	Protection rating	IP67
	Operating temperature (°C)	−10~40
	Climbing angle (°)	30
Nova 2	Weight of the unit (kg)	11
	Operating radius (mm)	625
	Payload (kg)	2
	Positioning accuracy (mm)	±0.05
	Protection rating	IP67

2.4. End Effector Design

The end effector is the core executing component of the intelligent transplanting robot for multi-variety rice seedlings, which directly contacts the rice seedlings to complete grasping and planting actions. Its structural design and control strategy determine the transplanting success rate, rice seedling damage rate, and multi-variety adaptability.

During manual transplanting, the operator coordinates the thumb, index finger, and middle finger to form an incomplete conical grasping space, thereby completing the precise grasping and planting of rice seedlings. This action not only ensures grasping stability but also minimizes damage to the root system. In this study, the bionic grasping posture of three-finger coordination was simplified into a two-finger structure obtained by symmetrically splitting a circular truncated cone, as shown in Figure 3a, with a maximum opening–closing stroke of S_{max} = 66 mm. The inner surface of each gripping finger was designed with a right-angled trapezoidal cross-section matching the natural morphology of the rice seedling bundle, as shown in Figure 3c (L_1 = 70 mm, L_2 = 20 mm, H = 106 mm). The oblique edge closely conforms to the naturally fluffy morphology of the rice seedling bundle, facilitating insertion into the soil; the right-angled edge precisely controls the grasping range through the symmetric opening–closing stroke, ensuring a stable number of seedlings picked per hill.

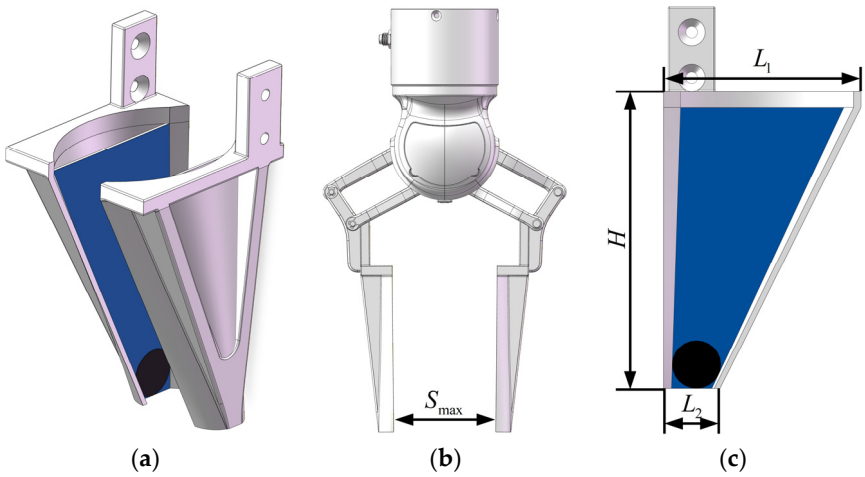


Figure 3. End effector design: (**a**) two-finger structure of the end effector; (**b**) end effector in the fully opened state; (**c**) inner surface of a single gripping finger.

To balance grasping strength and low-damage requirements, the end effector adopts a rigid–flexible coupling structure consisting of an "external rigid skeleton + internal flexible gripping layer," which are reliably connected through embedded T-shaped slots. The rigid skeleton is made of aluminum alloy, offering the advantages of light weight, high strength, and corrosion resistance; it not only ensures the structural stability of the end effector but also provides sufficient soil penetration strength to adapt to the complex working conditions in paddy fields. The flexible gripping layer is made of silicone, whose elastic deformation disperses the grasping stress and reduces relative sliding through flexible contact with the stems and roots of rice seedlings. It also compensates for the differences in stem thickness and root size among rice seedling varieties, thereby achieving multi-variety adaptability.

Meanwhile, to prevent the seedlings from falling off during transplanting and to avoid root damage, a force–position closed-loop control system based on thin-film pressure sensors (Jinhua Qisu Technology Co., Ltd., Jinhua, China) was constructed in this study to achieve precise sensing and dynamic regulation of the grasping force. The grasping force of the end effector must satisfy the following condition: the friction force generated by grasping must be greater than or equal to the sum of the total gravity of the seedlings and the vertical pulling force. Calculation of the clamping force first requires determining the coefficient of static friction between the flexible silicone gripping layer and the rice seedlings. In this study, the inclined-plane method was adopted to measure it, and the measurement principle is shown in Figure 4.

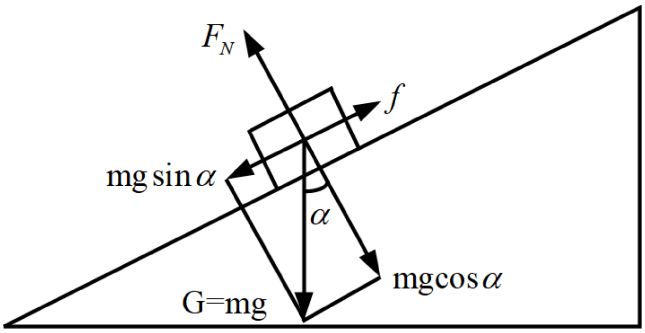


Figure 4. Schematic of the force analysis for measuring the friction coefficient by the inclined plane method.

As shown in Figure 4:

$$\mu = \frac{f}{F_N} = \frac{mg\sin\alpha}{mg\cos\alpha} = \tan\alpha \tag{1}$$

From the above equation, the coefficient of static friction μ between the silicone and the rice seedlings was calculated to be 0.55–0.67. To ensure that no slipping occurs even under the worst-case contact condition, the minimum value of the measured range, 0.55, was used for the clamping-force design. In addition, to compensate for uncertainties such as individual differences among seedlings, load fluctuations, and wear of the gripping surfaces, a safety factor of 2 was adopted following the general principles of gripper design. Based on the static friction principle, the grasping force was derived as follows:

$$F = \frac{n(mg + F_d)K}{2\mu} \tag{2}$$

where F is the total gripping force required by the end effector, N; n is the maximum number of seedlings per hole, taken as 5; m is the weight of a single plant with soil, kg; g is the

acceleration due to gravity, m/s^2; F_d is the vertical pull force per plant, N; K is the safety factor, taken as 2; μ is the coefficient of static friction between silicone and rice seedlings, taken as 0.55.

According to the above formula, the grasping force of the end effector for grasping rice seedlings was determined to be 1.3 N. Based on the principle of force interaction, the grasping pressure threshold of the end effector was calibrated as 1.3 N. Meanwhile, the thin-film pressure sensor was attached to the contact area between the internal flexible silicone of the end effector and the roots of the rice seedlings to collect grasping force data in real time. A force–position control strategy was constructed to achieve precise sensing and closed-loop regulation of the grasping force, whose workflow is shown in Figure 5.

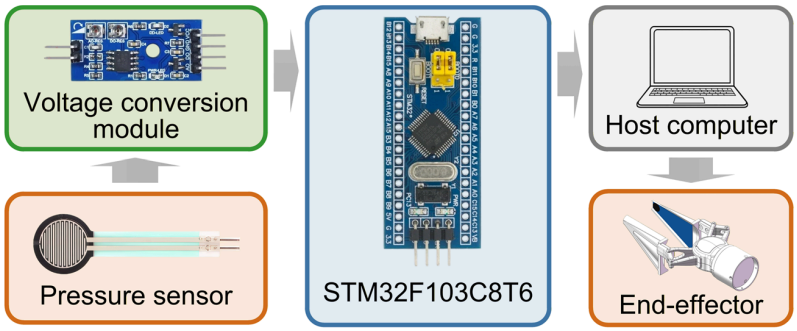


Figure 5. Workflow of the pressure sensor.

When the end effector performs a grasping action, the pressure sensor converts the physical pressure signal into a resistance change, which is linearly converted into a standard analog voltage signal by a voltage conversion module. The analog-to-digital converter (ADC) integrated in the STM32F103C8T6 microcontroller (STMicroelectronics, Geneva, Switzerland) completes analog-to-digital conversion; after filtering and calibration, the digital value is converted into the actual pressure value and uploaded to the host computer. The robot operating system (ROS) on the host computer parses the data and dynamically compares the real-time pressure value with the preset threshold. When the grasping force is detected to reach the threshold, a command is immediately sent to the main control system of the robotic arm to terminate the closing action of the end effector.

The pressure variation during the actual grasping process, measured by the pressure sensor, is shown in Figure 6. The actual clamping force fluctuates within a small range of 1.28–1.35 N, indicating that the system has good response speed and control accuracy.

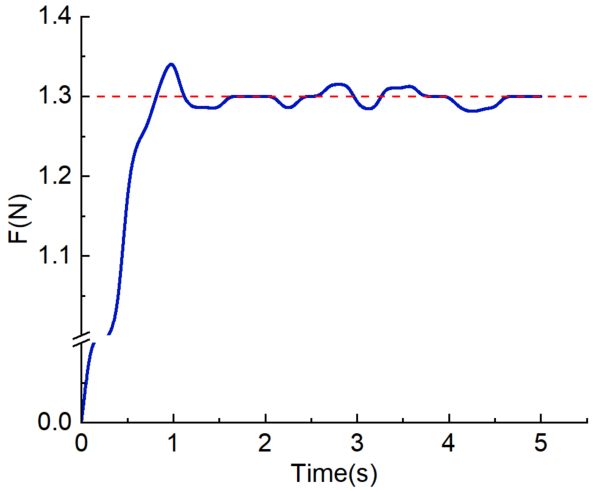


Figure 6. Pressure variation curve.

2.5. Design of the Visual Recognition and Positioning System

In this study, the You Only Look Once version 5s (YOLOv5s) object detection algorithm—the most lightweight member of the currently mature and stable YOLOv5 series—was selected for multi-variety rice seedling recognition. This algorithm offers the core advantages of fast detection speed and excellent real-time performance, imposes low requirements on the computing platform, and is easy to deploy on the robot platform, while its detection accuracy shows no significant loss compared with other versions of YOLOv5 [25,26]. During the research, several inherent difficulties were identified in this recognition task, as detailed below:

(1) Low inter-variety feature discriminability. At the seedling stage, different rice varieties show minimal morphological differences and lack distinctive recognition markers. Feature homogenization makes it difficult to extract variety-specific discriminative features, which easily leads to misclassification and missed detection, substantially increasing the detection difficulty.

(2) Prominent target distribution and occlusion problems. After tray raising, rice seedlings are densely and irregularly arranged, with slender leaves interlacing and causing severe occlusion and overlap. Since the operation requires precise grasping of a quantitative number of rice seedlings, occlusion blurs target boundaries and causes feature loss, substantially increasing the difficulty of model recognition, counting, and grasping.

Since this study focuses on the precision and damage-free control of the intelligent transplanting robot for multi-variety rice seedlings, auxiliary markers were adopted in the visual positioning stage to isolate perception errors; marker-free recognition in complex scenarios will be addressed in future work. Accordingly, distinct-color square labels were placed at fixed positions in front of the seedling trays to simplify recognition. Considering the solar irradiance during transplanting and to avoid color loss caused by camera overexposure under strong light, red, blue, yellow, and black—colors with high saturation, low lightness, and markedly different hues—were selected as the marker colors. It should be noted that the actual detection target of the vision system in this study is the artificial color-coded markers rather than the seedlings themselves: each variety is assigned a fixed marker color, and the variety identity and tray position are jointly determined by the preset "marker–variety" correspondence and the detected marker position.

Images under different lighting intensities simulated by lamps were collected using the depth camera. Data augmentation was performed by randomly rotating images at multiple angles, altering sharpness, saturation, and contrast, and adding noise. The training parameters are listed in Table 3, and the mean average precision (mAP) of the training results is shown in Figure 7. During training, there were slight fluctuations that gradually diminished in the later stage; the mAP increased gradually from approximately 74% and finally converged stably at 95.8%.

Table 3. Training parameters.

Parameters	Value
Input size	640 × 480
Number of images	400
Dataset split (training/validation/test)	8:1:1
Batch size	16
Epochs	200
Optimizer	SGD
Initial learning rate	0.01
Weight decay	0.0005
Momentum	0.937

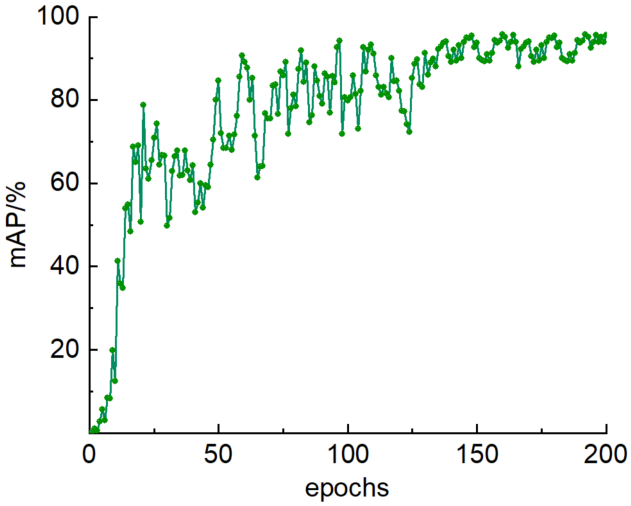


Figure 7. Variation curve of the mAP.

The results on the test set are listed in Table 4, indicating that the model has good stability and can meet the accuracy requirements for field recognition of rice seedlings.

Table 4. Quantitative metrics on the test set.

Parameters	Value
Precision	91.05%
Recall	90.59%
mAP@50	95.07%
mAP@50:0.95	49.71%
Inference speed	13.5 ms/image

The results of this study verify the feasibility of marker-assisted multi-variety recognition and localization under a controlled breeding workflow and should not be generalized to a complete marker-free multi-variety recognition solution. A qualitative analysis of the robustness of the marker recognition system under different working conditions is provided below, taking into account the system design and data acquisition approach. Light intensity: The training data were acquired under multiple light intensities simulated with artificial lighting, and data augmentation such as saturation and contrast adjustment and noise addition was applied to improve lighting adaptability. In addition, the markers were chosen in colors with high saturation, low brightness, and a hue significantly different from that of the green seedlings; together with camera exposure control, this avoids overexposure and color loss under strong light. Background conditions: The red, blue, yellow, and black markers are clearly separated in hue from the predominantly green seedlings, brown soil, and water-surface background, which inherently reduces background interference and the probability of false detection. The discrimination of black markers against a dark background can be compensated by verifying the shape feature of the square outline. Camera viewpoint: The data augmentation includes random rotation at multiple angles, and in actual operation the eye-in-hand camera approaches the tray in a near-fixed, near-vertical posture, so the viewpoint remains within a controlled range. Marker occlusion: The markers are mounted at a fixed position in front of the tray rack, and the degree of occlusion is limited under the standardized workflow, so recognition reliability can be maintained even under partial marker occlusion.

In this study, a binocular structured-light depth-sensing camera, the DaBai DC1 (Orbbec Inc., Shenzhen, China), was employed. The homogeneous transformation matrix from the camera coordinate frame of depth camera 1 to the end effector coordinate frame of

the robotic arm was determined through hand–eye calibration in an eye-in-hand configuration. The transformation matrix from the camera coordinate frame of depth camera 2 to the coordinate frame of the mobile chassis was obtained from the existing calibration parameters in the robot model; this known transformation was directly adopted without performing a separate calibration [27].

A 9 × 12 checkerboard calibration board with a single-square side length of 20 mm was used, and the board remained fixed during calibration. The robotic arm was controlled to move so that the camera captured images at different poses, yielding a total of 30 checkerboard images and 30 corresponding sets of end effector poses. For each image, the pose of the calibration board relative to the camera coordinate system was solved based on the checkerboard corner points. Combined with the pose of the end effector relative to the base coordinate system provided by the forward kinematics of the robotic arm, and according to the hand–eye calibration equation:

$$AX = XB \tag{3}$$

Combined with the pose of the end effector relative to the base coordinate system provided by the forward kinematics of the robotic arm, the hand–eye matrix T of the camera relative to the end of the robotic arm was solved according to the hand–eye calibration equation. The target pose measured in the camera coordinate system was then mapped to the base coordinate system of the robotic arm through the end effector coordinate system, providing reliable pose guidance for the precise transplanting motion planning of the robotic arm.

$$T = \begin{bmatrix} -0.8799 & -0.3383 & -0.3337 & -0.3786 \\ 0.4311 & -0.8637 & -0.2611 & 1.9816 \\ -0.1999 & -0.3736 & 0.9058 & -0.3661 \\ 0 & 0 & 0 & 1 \end{bmatrix} \tag{4}$$

2.6. Kinematics Analysis

The core research scope of robot kinematics is the mapping relationship between the position and orientation of the end effector and the joint-space variables of the robotic arm [28]. In this section, the forward and inverse kinematics equations of the robot are solved and the workspace of the robotic arm is analyzed, providing a solid theoretical basis for the precise motion control of the robotic arm and the execution of transplanting operations.

2.6.1. Forward Kinematics Analysis

The standard Denavit–Hartenberg (D-H) parameter method was used to establish the kinematic model of the robotic arm of the intelligent transplanting robot for multi-variety rice seedlings, and the coordinate systems at each joint are shown in Figure 8. According to the link parameters and the established coordinate systems, the D-H parameters of each joint were determined, as listed in Table 5 [29].

Table 5. Standard D-H parameters.

i	θ_i (°)	d_i (mm)	a_i (mm)	α_i (°)	Range of Motion (°)
1	θ_1	d_1 = 223.4	0	90	±360
2	θ_2	0	a_2 = 280	0	±180
3	θ_3	0	a_3 = 225	0	±156
4	θ_4	d_4 = 117.5	0	90	±360
5	θ_5	d_5 = 122	0	−90	±360
6	θ_6	d_6 = 88	0	0	±360

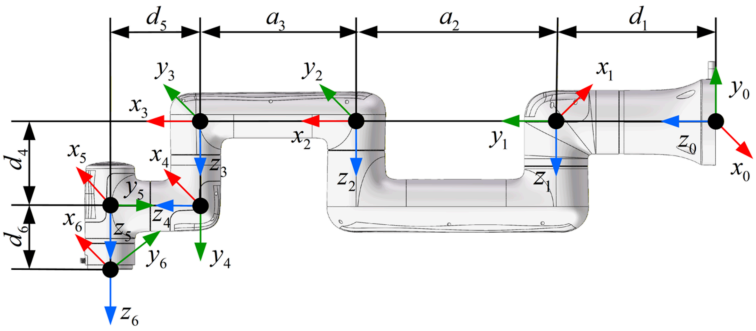


Figure 8. Link coordinate systems of the robotic arm.

The transformation matrix between adjacent link coordinate systems is:

$$\begin{aligned} {}^{i-1}_{i}T &= Rot(\theta_i)Trans(d_i)Trans(a_i)Rot(\alpha_i) \\ &= \begin{bmatrix} c\theta_i & -s\theta_i c\alpha_i & s\theta_i s\alpha_i & a_i c\theta_i \\ s\theta_i & c\theta_i c\alpha_i & -c\theta_i s\alpha_i & a_i s\theta_i \\ 0 & s\alpha_i & c\alpha_i & d_i \\ 0 & 0 & 0 & 1 \end{bmatrix} \end{aligned} \tag{5}$$

where $c\theta_i = cos\theta_i$, $s\theta_i = sin\theta_i$, $c\alpha_i = cos\alpha_i$, $s\alpha_i = sin\alpha_i$.

The transformation matrix ${}^{0}_{6}T$ of the end effector relative to the base coordinate system of the robotic arm of the intelligent transplanting robot for multi-variety rice seedlings is:

$${}^{0}_{6}T = {}^{0}_{1}T\,{}^{1}_{2}T\,{}^{2}_{3}T\,{}^{3}_{4}T\,{}^{4}_{5}T\,{}^{5}_{6}T = \begin{bmatrix} n_x & o_x & a_x & p_x \\ n_y & o_y & a_y & p_y \\ n_z & o_z & a_z & p_z \\ 0 & 0 & 0 & 1 \end{bmatrix} \tag{6}$$

where the 12 effective elements of ${}^{0}_{6}T$ are:

$$\begin{cases} n_x = c_6(s_1s_5 + c_1c_5c_{234}) - c_1s_6s_{234} \\ n_y = -c_6(c_1s_5 - c_5s_1c_{234}) - s_1s_6s_{234} \\ n_z = s_6c_{234} + c_5c_6s_{234} \\ o_x = -s_6(s_1s_5 + c_1c_5c_{234}) - c_1c_6s_{234} \\ o_y = s_6(c_1s_5 - c_5s_1c_{234}) - c_6s_1s_{234} \\ o_z = c_6c_{234} - c_5s_6s_{234} \\ a_x = c_5s_1 - c_1s_5c_{234} \\ a_y = -c_1c_5 - s_1s_5c_{234} \\ a_z = -s_5s_{234} \\ p_x = d_4s_1 + d_6(c_5s_1 - c_1s_5c_{234}) + c_1d_5s_{234} + a_2c_1c_2 - a_3c_1(s_2s_3 + c_2c_3) \\ p_y = d_5s_1s_{234} - d_6(c_1c_5 + s_1s_5c_{234}) - c_1d_4 + a_2c_2s_1 - a_3s_1(s_2s_3 + c_2c_3) \\ p_z = d_1 - d_5c_{234} + a_2s_2 + a_3s_{23} - d_6s_5s_{234} \end{cases} \tag{7}$$

where $c_i = cos\theta_i$, $s_i = sin\theta_i$, $c_{234} = cos(\theta_2 + \theta_3 + \theta_4)$, $s_{234} = sin(\theta_2 + \theta_3 + \theta_4)$, $c_{23} = cos(\theta_2 + \theta_3)$, $s_{23} = sin(\theta_2 + \theta_3)$.

2.6.2. Inverse Kinematics Analysis

The core of the inverse kinematics of the robotic arm is to inversely solve the joint rotation angles, given the target pose of the end effector relative to the base coordinate

system, thereby achieving precise end positioning and trajectory control through joint motion. It is the key technical foundation for ensuring that the intelligent transplanting robot for multi-variety rice seedlings stably completes core operations such as grasping, transporting, and planting [30].

The Dobot Nova 2 collaborative robotic arm satisfies the Pieper criterion, as its three wrist axes intersect at a single point; therefore, its inverse kinematics admits a closed-form analytical solution, offering the advantages of smooth control and high positioning accuracy [31]. Therefore, the algebraic method among the analytical approaches was adopted in this study to solve the inverse kinematics of the robotic arm of the intelligent transplanting robot for multi-variety rice seedlings, so as to meet the requirements of transplanting operations for high real-time performance, high positioning accuracy, and high operational stability.

Multiply both sides of ${}_{6}^{0}T$ by ${}_{1}^{0}T^{-1}$ from the left:

$$ {}_{1}^{0}T^{-1}{}_{6}^{0}T = {}_{2}^{1}T{}_{3}^{2}T{}_{4}^{3}T{}_{5}^{4}T{}_{6}^{5}T \tag{8} $$

According to Equation (8), the elements in corresponding positions of the matrices on both sides of the equation are equal:

$$ (d_6 a_y - p_y)c_1 - (a_x d_6 - p_x)s_1 = d_4 \tag{9} $$

Order $m_1 = d_6 a_y - p_y$, $n_1 = a_x d_6 - p_x$:

$$ \theta_1 = A\tan 2(m_1, n_1) - A\tan 2\left(d_4, \pm\sqrt{m_1^2 + n_1^2 - d_4^2}\right) \tag{10} $$

According to Equation (8), the elements in corresponding positions of the matrices on both sides of the equation are equal:

$$ a_x s_1 - a_y c_1 = c_5 \tag{11} $$

The solution is:

$$ \theta_5 = \pm\arccos(a_x s_1 - a_y c_1) \tag{12} $$

According to Equation (8), the elements in corresponding positions of the matrices on both sides of the equation are equal:

$$ s_6(o_y c_1 - o_x s_1) - c_6(n_y c_1 - n_x s_1) = s_5 \tag{13} $$

Order $m_6 = o_y c_1 - o_x s_1$, $n_6 = n_y c_1 - n_x s_1$:

$$ \theta_6 = A\tan 2(m_6, n_6) - A\tan 2\left(s_5, \pm\sqrt{m_6^2 + n_6^2 - s_5^2}\right) \tag{14} $$

Multiply both sides of ${}_{6}^{0}T$ by ${}_{1}^{0}T^{-1}$ on the left and by ${}_{6}^{5}T^{-1}{}_{5}^{4}T^{-1}$ on the right simultaneously:

$$ {}_{1}^{0}T^{-1}{}_{6}^{0}T{}_{6}^{5}T^{-1}{}_{5}^{4}T^{-1} = {}_{2}^{1}T{}_{3}^{2}T{}_{4}^{3}T \tag{15} $$

According to Equation (15), the elements in corresponding positions of the matrices on both sides of the equation are equal:

$$ \begin{cases} d_5\left[s_6\left(n_x c_1 + n_y s_1\right) + c_6\left(o_x c_1 + o_y s_1\right)\right] - d_6\left(a_x c_1 + a_y s_1\right) + p_x c_1 + p_y s_1 = a_3 c_{23} + a_2 c_2 \\ p_z - d_1 - a_z d_6 + d_5(o_z c_6 + n_z s_6) = a_3 s_{23} + a_2 s_2 \end{cases} \tag{16} $$

Order:

$$\begin{cases} d_5\left[s_6\left(n_x c_1 + n_y s_1\right) + c_6\left(o_x c_1 + o_y s_1\right)\right] - d_6\left(a_x c_1 + a_y s_1\right) + p_x c_1 + p_y s_1 = m_3 \\ p_z - d_1 - a_z d_6 + d_5(o_z c_6 + n_z s_6) = n_3 \end{cases} \tag{17}$$

Substituting m_3, n_3 into Equation (16):

$$\begin{cases} m_3 = a_3 c_{23} + a_2 c_2 \\ n_3 = a_3 s_{23} + a_2 s_2 \end{cases} \tag{18}$$

Find the sum of the squares of m_3, n_3:

$$c_3 = \frac{m_3^2 + n_3^2 - a_2^2 - a_3^2}{2a_2 a_3} \tag{19}$$

The solution is:

$$\theta_3 = \pm \arccos\left(\frac{m_3^2 + n_3^2 - a_2^2 - a_3^2}{2a_2 a_3}\right) \tag{20}$$

Rewrite Equation (18):

$$\begin{cases} s_2 = \frac{(a_3 c_3 + a_2) n_3 - a_3 s_3 m_3}{a_2^2 + a_3^2 + 2a_2 a_3 c_3} \\ c_2 = \frac{m_3 + a_3 s_3 s_2}{a_3 c_3 + a_2} \end{cases} \tag{21}$$

The solution is:

$$\theta_2 = A \tan 2(s_2, c_2) \tag{22}$$

Multiply both sides of ${}_6^0T$ by ${}_1^0T^{-1}$ on the left and by ${}_6^5T^{-1}$ on the right simultaneously:

$$\begin{cases} s_6\left(n_x c_1 + n_y s_1\right) + c_6\left(o_x c_1 + o_y s_1\right) = -s_{234} \\ o_z c_6 + n_z s_6 = c_{234} \end{cases} \tag{23}$$

Order:

$$\begin{cases} s_6\left(n_x c_1 + n_y s_1\right) + c_6\left(o_x c_1 + o_y s_1\right) = m_4 \\ o_z c_6 + n_z s_6 = n_4 \end{cases} \tag{24}$$

The solution is:

$$\theta_4 = A \tan 2(-m_4, n_4) - \theta_2 - \theta_3 \tag{25}$$

2.6.3. Workspace Analysis

The robot workspace refers to the spatial range that the end reference point of the robot can reach in the base coordinate system, and its shape and size have a critical influence on the working performance of the robot when performing operational tasks [32]. In this study, the Monte Carlo method was used to obtain an approximate solution of the workspace. Based on the kinematic model in the MATLAB Robotics Toolbox (MathWorks Inc., Natick, MA, USA), 60,000 joint-angle points were randomly sampled and calculated according to the actual joint ranges of the robotic arm, and the pose was obtained through the forward kinematics solution [33]. The results are shown in Figure 9.

As shown in Figure 9, neglecting the interference of other structures on the motion of the robotic arm, the projected points of the theoretical workspace in the three planes are uniformly distributed, and the overall spatial contour is approximately spherical, with no obvious motion blind zones or unreachable areas. According to the working conditions

of rice seedling transplanting, the core working area of the robotic arm is divided into a grasping area and a planting area. Accordingly, the grasping and planting actions require the end effector to maintain a vertically downward orientation constraint, which requires the axis of the sixth joint to be synchronously perpendicular to the plane. Therefore, the radius of the robot's actual grasping workspace (537 mm) was obtained by subtracting the length of the sixth link from the theoretical workspace radius of the manipulator (625 mm); that is, the grasping workspace is the interior of a circle whose radius is the distance from the farthest working point reachable in the grasping posture, shown in Figure 10, to the rotational axis of the manipulator's first joint. The radius of the robot's actual planting workspace (800 mm) was obtained by adding the height of the end effector to the actual grasping workspace radius; that is, the planting workspace is the interior of a circle whose radius is the distance from the farthest working point reachable in the planting posture, shown in Figure 10, to the rotational axis of the manipulator's first joint.

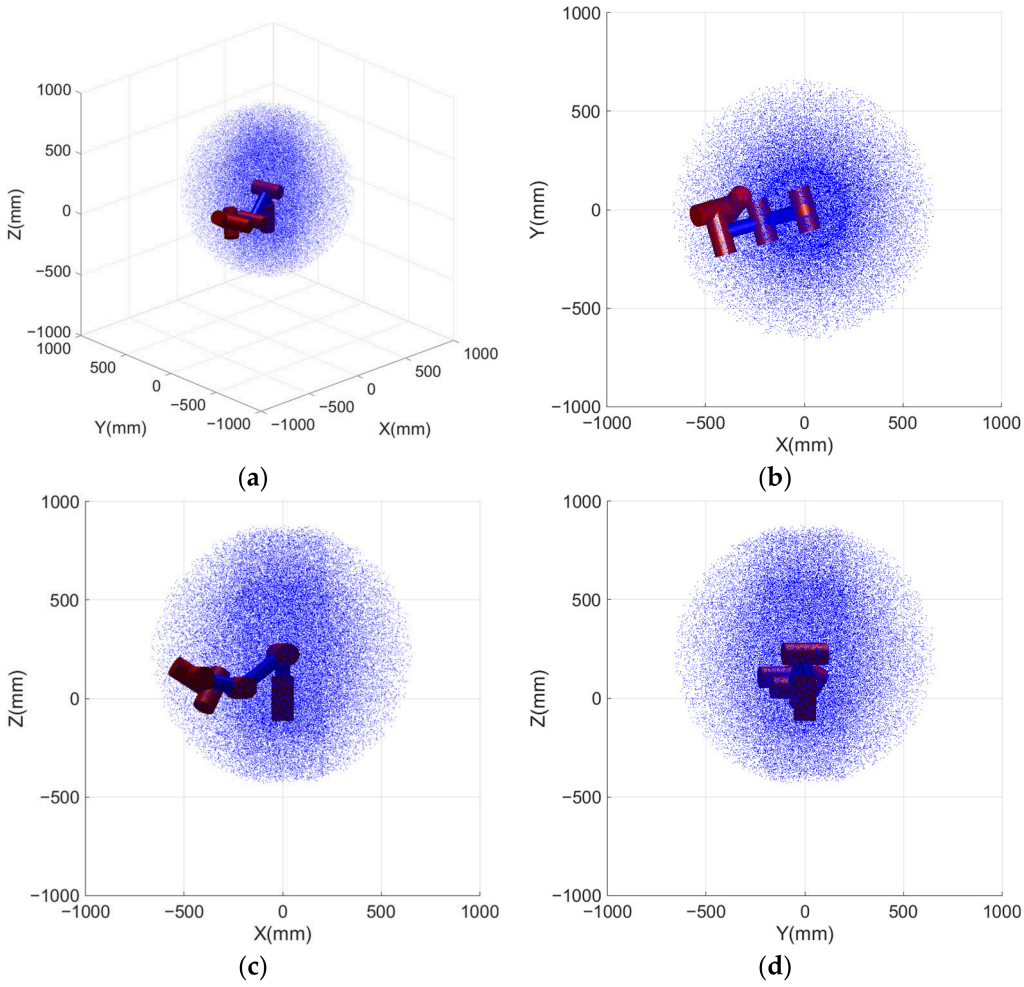


Figure 9. Workspace distribution of the robotic arm: (**a**) three-dimensional view; (**b**) XY plane; (**c**) XZ plane; (**d**) YZ plane.

As shown in Figure 10, the farthest grasping and planting working points, verified by the MATLAB model and mapped onto the three-dimensional model, lie within the joint limits, are not singular configurations, and involve no mechanical interference. All equivalent simulation models of rice seedlings are within the actual grasping workspace, and the actual planting workspace extends well beyond the lowest edge of the mobile chassis, indicating that both the grasping and planting areas are fully contained within

the robot's actual workspace and satisfy the full-stroke reachability requirement of the transplanting operation.

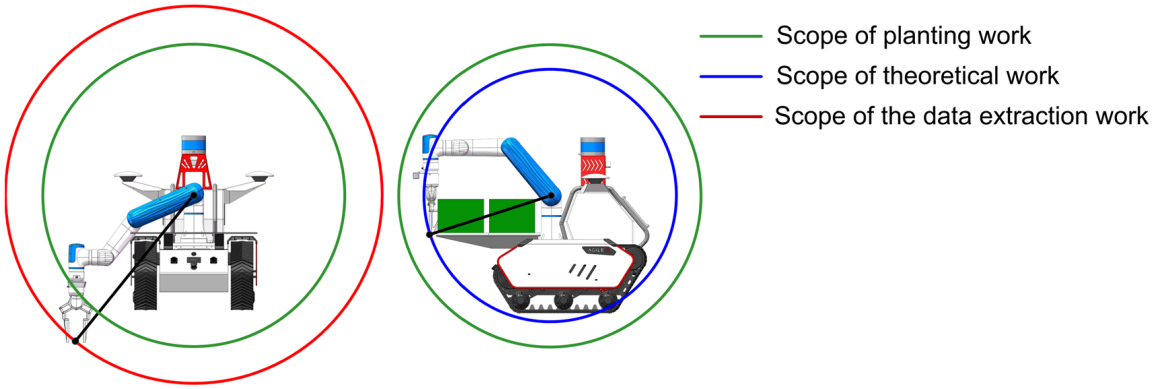


Figure 10. Actual workspace of the intelligent transplanting robot for multi-variety rice seedlings.

3. Results

To verify the transplanting performance of the intelligent transplanting robot for multi-variety rice seedlings, a test platform excluding the autonomous driving function of the mobile chassis was built, as shown in Figure 11, which mainly includes a BUNKER MINI mobile chassis, a Nova 2 robotic arm, an end effector, a depth camera, and a host computer. A laser rangefinder and a microscope were employed as auxiliary instruments for accuracy measurement and damage inspection. The damage rate, transplanting accuracy rate, transplanting success rate, and average transplanting cycle time per hill were taken as the evaluation metrics, defined as follows:

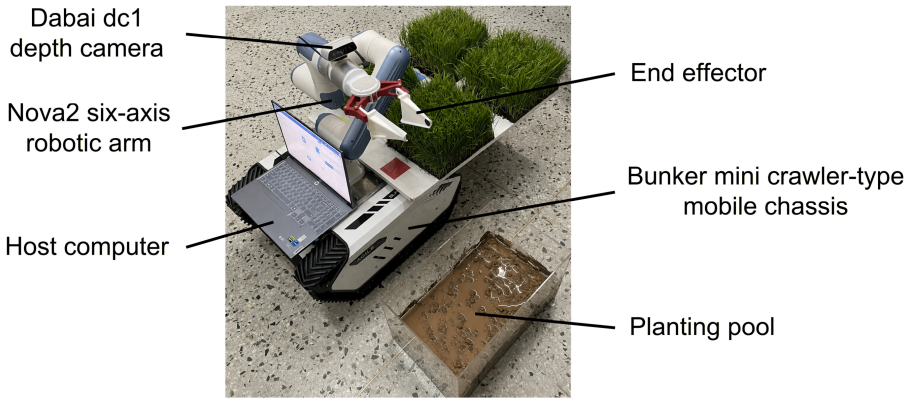


Figure 11. Test bench for multi-variety rice seedling transplanting.

Damage rate: the ratio of the number of seedlings with a root breakage length $\geq 1/3$ of the total root length or a fractured stem to the total number of transplanted seedlings, calculated as:

$$D = \frac{N_D}{N} \times 100\% \tag{26}$$

Transplanting accuracy rate: the ratio of seedlings whose row spacing, plant spacing, and transplanting depth all meet the specified requirements and whose seedling count per hill lies within the specified range to the total number of transplanted seedlings, calculated as:

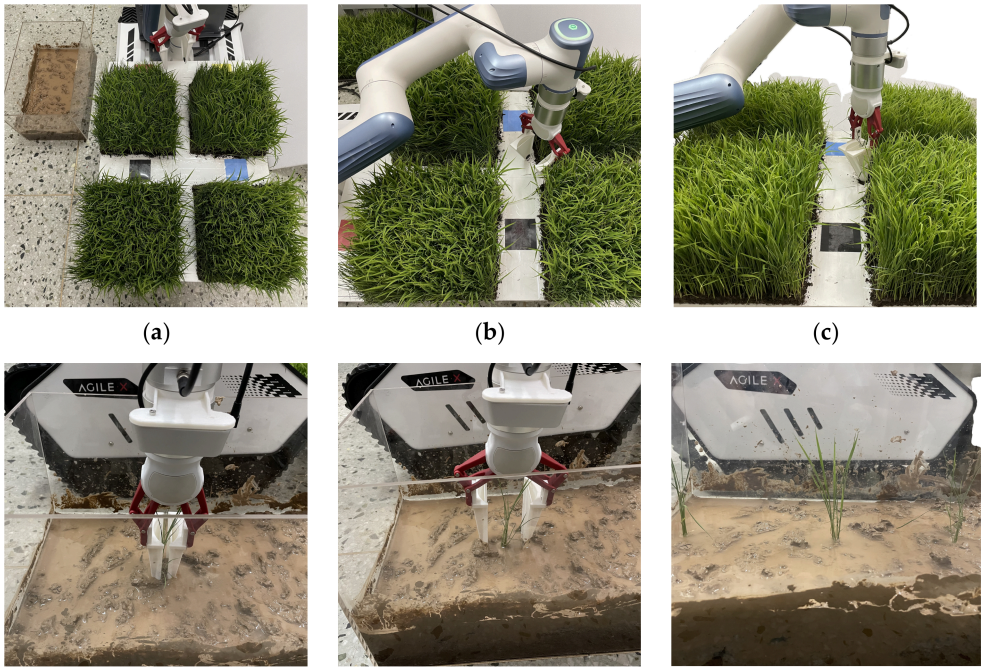
$$A = \frac{N_A}{N} \times 100\% \tag{27}$$

Transplanting success rate: the ratio of seedlings that are free of damage and meet the accuracy requirements to the total number of transplanted seedlings, calculated as:

$$S = \frac{N_S}{N} \times 100\% \tag{28}$$

where N is the total number of transplanted seedlings; N_D is the number of damaged seedlings; N_A is the number of seedlings transplanted accurately; N_S is the number of seedlings transplanted successfully; D is the damage rate; A is the transplanting accuracy rate; and S is the transplanting success rate.

The transplanting experiment was conducted on 13 May 2026. Based on the multi-variety rice seedling transplanting test platform whose parameters matched those of the breeding experimental fields in the Jiansanjiang Reclamation Area of Heilongjiang, four rice seedling varieties at the experimental stages, labeled A, B, C, and D, were randomly selected. According to the agronomic parameters of rice seedling transplanting and the mechanical transplanting standards, and following the transplanting workflow, multi-variety rice seedling transplanting experiments were conducted in the current working area. The specific transplanting process is shown in Figure 12, and the transplanting results are listed in Table 6.



(**a**) (**b**) (**c**)

(**d**) (**e**) (**f**)

Figure 12. The transplanting trial process: (**a**) The robotic arm moves to its initial position and performs visual recognition and positioning, (**b**) the robotic arm moves to the pickup point, (**c**) the end effector closes and stops closing when the pressure reaches the threshold, (**d**) the robotic arm moves to the planting point, (**e**) end effector open, (**f**) transplanting results.

Table 6. Transplanting experiment results of the four rice seedling varieties.

Variety	A	B	C	D	Inter-Group Test	Total	95% Wilson Confidence Interval
Number of seedlings per hole (plant)	4~6	4~5	4~5	5~6	H = 4.30, p = 0.231	/	/
Average row spacing (cm)	30.20 ± 0.22	29.70 ± 0.10	30.10 ± 0.21	30.10 ± 0.40	F = 3.71, p = 0.034	/	/
Average plant spacing (cm)	13.10 ± 0.12	12.90 ± 0.25	13.20 ± 0.16	13.00 ± 0.12	F = 2.78, p = 0.075	/	/

Table 6. *Cont.*

Variety	A	B	C	D	Inter-Group Test	Total	95% Wilson Confidence Interval
Average transplanting depth (cm)	2.15 ± 0.20	1.72 ± 0.14	1.58 ± 0.07	2.02 ± 0.11	F = 17.68, $p < 0.001$	/	/
Single-hill transplanting time (s)	6.98 ± 0.03	7.39 ± 0.06	9.75 ± 0.04	7.28 ± 0.04	F = 4070, $p < 0.001$	/	/
Number of transplanted seedlings (plant)	24	24	23	27	/	98	/
Number of damaged seedlings (plant)	1	1	0	1	/	3	/
Number of Accurately Transplanted Seedlings (plant)	23	24	23	26	/	96	/
Number of successfully transplanted seedlings (plant)	22	23	23	25	/	93	/
Damage rate (%)	4.17	4.17	0	3.70	/	3.06	1.05~8.62
Transplanting Accuracy Rate (%)	95.83	100	100	96.30	/	97.96	92.86~99.44
Transplanting success rate(%)	91.67	95.83	100	92.59	/	94.90	88.61~97.80

4. Discussion

In this study, an intelligent transplanting robot for multi-variety rice seedlings adapted to the operational requirements of breeding experimental fields was designed, and its operational performance was verified through theoretical analysis and experiments. The overall transplanting success rate reached 94.90%, and the success rate of each variety was above 91.67%, indicating that the robot has stable performance and good multi-variety adaptability.

Benefiting from the millimeter-level positioning accuracy of the robotic arm, the overall transplanting accuracy rate in the experiment reached 97.96%. The row spacing and plant spacing of the robot-transplanted seedlings exhibited high stability and were well within the allowable agronomic tolerances. Regarding transplanting depth, the slight slope of the planting surface caused relatively large fluctuations in depth, but the values remained within the standard range of 2 ± 0.5 cm; this will be further improved in future work by introducing closed-loop control of transplanting depth. The number of seedlings per hill was generally controlled at 4–6, essentially meeting the requirement of 4 ± 1. Slight exceedances occurred in a few varieties owing to differences in seedling density and minor root entanglement, which did not cause seedling damage and had a limited effect on the experimental data. In subsequent work, a vibration device can be installed at the bottom of the seedling tray rack to pre-separate the entangled roots through low-frequency vibration.

The overall average damage rate was only 3.06%. The differences in damage rate among varieties were mainly caused by the distinct physical characteristics of the rice seedlings. As shown in Figure 13, the core cause of damage was excessive root entanglement between adjacent seedlings: when the end effector grasped the seedlings, it could not precisely separate the independent root systems of adjacent seedlings, causing fracture damage to the roots of severely entangled seedlings. Moreover, the more developed the root system, the more tightly the roots were entangled, and the more severe the damage.

In terms of operational efficiency, the experimentally measured single-hill transplanting time of each variety ranged from 6.98 to 9.75 s, with an average single-hill transplanting time of 7.85 s. This duration covers the complete operation cycle of "recognition–grasping–transporting–planting–reset." On the premise of ensuring transplanting precision and

low damage, this operation tempo can meet the continuous operation requirements of small-plot, multi-variety precision transplanting in breeding experimental fields. In future work, the single-hill operation cycle can be further shortened by optimizing the motion trajectory of the robotic arm and the time consumed by visual recognition.

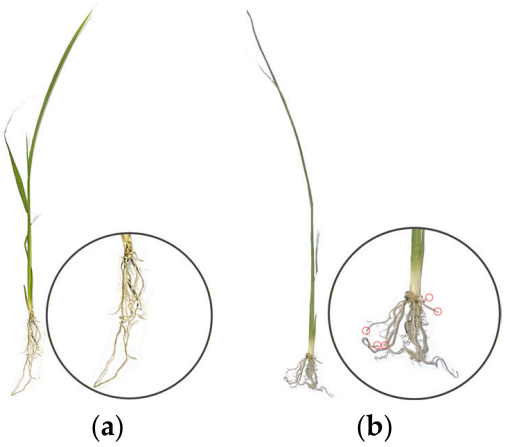


Figure 13. Examples of rice seedling damage: (**a**) undamaged rice seedlings; (**b**) damaged rice seedlings. The red circles indicate broken roots.

5. Conclusions

Targeting the specific operational requirements of rice breeding experimental fields, this study developed an intelligent transplanting robot for multi-variety rice seedlings, breaking through key technologies including low-damage grasping, precise recognition and positioning, and full-process automated cooperative control. The operational performance of the robot was verified through theoretical analysis and experiments, and the main conclusions are as follows:

(1) The rigid–flexible coupled end effector, designed based on the bionic principle of manual transplanting and combined with a force–position closed-loop control strategy, effectively solved the problem of poor grasping-force adaptability for multi-variety rice seedlings and achieved low-damage quantitative grasping. The experimental average damage rate was only 3.06%.

(2) Using a visual recognition scheme combining the YOLOv5s algorithm with distinct-color auxiliary markers, the model achieved a mean average precision of 95.8%. Together with the DaBai DC1 depth camera and eye-in-hand hand–eye calibration, precise acquisition of the three-dimensional pose of rice seedlings was realized, providing reliable guidance for the transplanting motion planning of the robotic arm.

(3) Based on the standard D-H parameter method, a kinematic model of the Nova 2 six-axis robotic arm was established, and a closed-form analytical inverse solution was obtained. The workspace was analyzed using the Monte Carlo method, and a geometric model of the actual working range was constructed, verifying that both the grasping and planting areas lie within the reachable range of the robot and satisfy the full-stroke requirements of transplanting operations.

Further research is still needed. In future work, the visual algorithm will be optimized to achieve marker-free precise recognition according to the morphological characteristics of multi-variety rice seedlings; the end effector will be improved with a root pre-separation device and the quantitative seedling-picking control strategy refined; and large-scale field validation experiments under multiple working conditions will be conducted to enhance the stability and versatility of the equipment.

Author Contributions: Conceptualization, C.K. and D.Y.; methodology, C.K. and D.Y.; software, C.K.; validation, C.K., Y.W. and R.Z.; formal analysis, C.K. and Q.Z.; investigation, Y.W., R.Z., Q.Z. and Z.S.; resources, Z.S. and D.Y.; data curation, C.K. and Y.W.; writing—original draft preparation, C.K.; writing—review and editing, D.Y., Z.S. and Q.Z.; visualization, C.K. and R.Z.; supervision, D.Y.; project administration, D.Y.; funding acquisition, D.Y. All authors have read and agreed to the published version of the manuscript.

Funding: This research received no external funding.

Data Availability Statement: The original contributions presented in this study are included in the article. Further inquiries can be directed to the corresponding author.

Conflicts of Interest: The authors declare no conflicts of interest.

Abbreviations

The following abbreviations are used in this manuscript:

ADC	Analog-to-digital converter
D-H	Denavit–Hartenberg
EKF	Extended Kalman filter
GNSS	Global navigation satellite system
IMU	Inertial measurement unit
IP67	Ingress protection 67
LiDAR	Light detection and ranging
mAP	Mean average precision
PID	Proportional–integral–derivative
ROS	Robot operating system
RTK	Real-time kinematic
SLAM	Simultaneous localization and mapping
YOLOv5s	You Only Look Once version 5s

References

1. Yuan, S.; Linquist, B.A.; Wilson, L.T.; Cassman, K.G.; Stuart, A.M.; Pede, V.; Miro, B.; Saito, K.; Agustiani, N.; Aristya, V.E.; et al. Sustainable Intensification for a Larger Global Rice Bowl. *Nat. Commun.* **2021**, *12*, 7163. [CrossRef]
2. Ladha, J.K.; Radanielson, A.M.; Rutkoski, J.E.; Buresh, R.J.; Dobermann, A.; Angeles, O.; Pabuayon, I.L.B.; Santos-Medellín, C.; Fritsche-Neto, R.; Chivenge, P.; et al. Steady Agronomic and Genetic Interventions Are Essential for Sustaining Productivity in Intensive Rice Cropping. *Proc. Natl. Acad. Sci. USA* **2021**, *118*, e2110807118. [CrossRef]
3. Yu, S.; Ali, J.; Zhang, C.; Li, Z.; Zhang, Q. Genomic Breeding of Green Super Rice Varieties and Their Deployment in Asia and Africa. *Theor. Appl. Genet.* **2020**, *133*, 1427–1442. [CrossRef]
4. Jyoti, S.D.; Singh, G.; Pradhan, A.K.; Tarpley, L.; Septiningsih, E.M.; Talukder, S.K. Rice Breeding for Low Input Agriculture. *Front. Plant Sci.* **2024**, *15*, 1408356. [CrossRef]
5. Kim, D.-H.; Jang, T.; Hwang, S.; Jeong, H. Paddy Rice Adaptation Strategies to Climate Change: Transplanting Date Shift and BMP Applications. *Agric. Water Manag.* **2021**, *252*, 106926. [CrossRef]
6. Liu, W.; Tian, S.; Wang, Q.; Jiang, H. Key Technologies of Plug Tray Seedling Transplanters in Protected Agriculture: A Review. *Agriculture* **2023**, *13*, 1488. [CrossRef]
7. Borda, Á.J.; Sárvári, B.; Balogh, J.M. Generation Change in Agriculture: A Systematic Review of the Literature. *Economies* **2023**, *11*, 129. [CrossRef]
8. Pitoyo, J. Development of Wide-Narrow Inter-Row Spacing Walking-Type Rice Transplanter in Indonesia. *J. Jpn. Soc. Agric. Mach. Food Eng.* **2020**, *82*, 117–119. [CrossRef]
9. Zhou, M.; Wang, G.; Zhang, Y.; Yang, J.; Wei, Z.; Sun, H.; Yin, J. Design and Test of Walk-Type Rice Potted Seedling Transplanting Machine. *Adv. Mech. Eng.* **2024**, *16*, 1–12. [CrossRef]
10. Ye, Y. Design and Field Validation of an Automated Sensor-Integrated High-Capacity Corn Plot Seeder. *Sci. Rep.* **2026**, *16*, 28029. [CrossRef]
11. Zhang, Y.; Xie, H.; Zhang, D.; Yang, L.; Lu, Z.; Cui, T.; He, X.; Zhang, K. Design and Experimental Study of Ridge-Grown Strawberry Automatic Harvesting Robot. *Comput. Electron. Agric.* **2026**, *240*, 111112. [CrossRef]

12. Oliveira, L.F.P.; Moreira, A.P.; Silva, M.F. Advances in Agriculture Robotics: A State-of-the-Art Review and Challenges Ahead. *Robotics* **2021**, *10*, 52. [CrossRef]
13. Zhu, D.; Shi, M.; Wang, Y.; Xue, K.; Liao, J.; Xiong, W.; Kuang, F.; Zhang, S. Path tracking control method for automatic navigation rice transplanters based on VUFC and improved BAS algorithm. *Robotica* **2023**, *41*, 3116–3136. [CrossRef]
14. Lohan, S.K.; Narang, M.K.; Raghuvirsinh, P.; Kumar, S.; Singh, L.P. Development and Field Evaluation of a VR/AR-based Remotely Controlled System for a Two-wheel Paddy Transplanter. *J. Field Robot.* **2024**, *41*, 2732–2748. [CrossRef]
15. Wu, W.; Zhang, Z.; Zhang, X.; He, Y.; Fang, H. Application of Visual Inertia Fusion Technology in Rice Transplanter Operation. *Comput. Electron. Agric.* **2024**, *221*, 108990. [CrossRef]
16. He, J.; Luo, X.; Zhang, Z.; Wang, P.; He, J.; Yue, B.; Ding, F.; Zhu, Q. Positioning Correction Method for Rice Transplanters Based on the Attitude of the Implement. *Comput. Electron. Agric.* **2020**, *176*, 105598. [CrossRef]
17. Siddique, M.A.A.; Kim, W.-S.; Kim, Y.-S.; Kim, T.-J.; Choi, C.-H.; Lee, H.-J.; Chung, S.-O.; Kim, Y.-J. Effects of Temperatures and Viscosity of the Hydraulic Oils on the Proportional Valve for a Rice Transplanter Based on PID Control Algorithm. *Agriculture* **2020**, *10*, 73. [CrossRef]
18. Zhou, M.; Yang, J.; Yin, J.; Wang, Z. Design Method and Experimental Study of a Rice Transplanting Mechanism with Three Planting Arms Constrained by Differential Noncircular Gear Trains. *J. Asabe* **2022**, *65*, 221–233. [CrossRef]
19. Kootstra, G.; Wang, X.; Blok, P.M.; Hemming, J.; van Henten, E. Selective Harvesting Robotics: Current Research, Trends, and Future Directions. *Curr. Robot. Rep.* **2021**, *2*, 95–104. [CrossRef]
20. Silwal, A.; Davidson, J.R.; Karkee, M.; Mo, C.; Zhang, Q.; Lewis, K. Design, Integration, and Field Evaluation of a Robotic Apple Harvester. *J. Field Robot.* **2017**, *34*, 1140–1159. [CrossRef]
21. Xiong, Y.; Peng, C.; Grimstad, L.; From, P.J.; Isler, V. Development and Field Evaluation of a Strawberry Harvesting Robot with a Cable-Driven Gripper. *Comput. Electron. Agric.* **2019**, *157*, 392–402. [CrossRef]
22. Yang, Q.; Qu, G.; Zhong, X.; Yang, X.; Liu, L.; Hu, X.; Addy, M.M. Design and Performance Evaluation of a Rigid-Flexible Coupling End-Effector for Tomato Picking Robots. *Eng. Agric.* **2026**, *13*, 25643. [CrossRef]
23. Zhang, L.; Wang, Z.; E, S.; Du, G.; Chen, Z. Analysis of Climatic Basis for the Change of Cultivated Land Area in Sanjiang Plain of China. *Front. Earth Sci.* **2022**, *10*, 862141. [CrossRef]
24. Zhou, M.; Sun, L.; Du, X.; Zhao, Y.; Xin, L. Optimal Design and Experiment of Rice Pot Seedling Transplanting Mechanism with Planetary Bezier Gears. *Trans. Asabe* **2014**, *57*, 1537–1548. [CrossRef]
25. Li, H.; Gu, Z.; He, D.; Wang, X.; Huang, J.; Mo, Y.; Li, P.; Huang, Z.; Wu, F. A Lightweight Improved YOLOv5s Model and Its Deployment for Detecting Pitaya Fruits in Daytime and Nighttime Light-Supplement Environments. *Comput. Electron. Agric.* **2024**, *220*, 108914. [CrossRef]
26. Chen, S.; Liu, J.; Xu, X.; Guo, J.; Hu, S.; Zhou, Z.; Lan, Y. Detection and Tracking of Agricultural Spray Droplets Using GSConv-Enhanced YOLOv5s and DeepSORT. *Comput. Electron. Agric.* **2025**, *235*, 110353. [CrossRef]
27. Yin, Y.; Gao, D.; Lu, Y.; Zhao, C.; Li, G.; Deng, K. In-Situ Robot Joint Stiffness Identification Using an Eye-in-Hand Camera with Optimal Measurement Pose Selection. *Measurement* **2025**, *253*, 117579. [CrossRef]
28. Fan, J.; Jin, L.; Xie, Z.; Li, S.; Zheng, Y. Data-Driven Motion-Force Control Scheme for Redundant Manipulators: A Kinematic Perspective. *IEEE Trans. Ind. Inform.* **2022**, *18*, 5338–5347. [CrossRef]
29. Yang, J.; Jin, L.; Han, Z.; Zhao, D.; Hu, M. Sensitivity Analysis of Factors Affecting Motion Reliability of Manipulator and Fault Diagnosis Based on Kernel Principal Component Analysis. *Robotica* **2022**, *40*, 2547–2566. [CrossRef]
30. Wang, S.; Liu, Z.; Ma, Z.; Chang, H.; Huang, P.; Lu, Z. A Closed-Form Solution for Inverse Kinematics of Redundant Space Manipulator with Multiple Joint Offsets. *Adv. Space Res.* **2023**, *72*, 1844–1860. [CrossRef]
31. Wang, H.; Lu, X.; Cui, W.; Zhang, Z.; Li, Y.; Sheng, C. General Inverse Solution of Six-Degrees-of-Freedom Serial Robots Based on the Product of Exponentials Model. *Assem. Autom.* **2018**, *38*, 361–367. [CrossRef]
32. Gupta, K.C. On the Nature of Robot Workspace. *Int. J. Robot. Res.* **1986**, *5*, 112–121. [CrossRef]
33. Wang, Z.; Hu, D.; Wan, D.; Liu, C. An Improved Inverse Kinematics Solution Method for the Hyper-redundant Manipulator with End-link Pose Constraint. *J. Field Robot.* **2024**, *41*, 1900–1921. [CrossRef]

Disclaimer/Publisher's Note: The statements, opinions and data contained in all publications are solely those of the individual author(s) and contributor(s) and not of MDPI and/or the editor(s). MDPI and/or the editor(s) disclaim responsibility for any injury to people or property resulting from any ideas, methods, instructions or products referred to in the content.